Differential surface photovoltage spectroscopy characterization of a 1.3 μm InGaAlAs/InP vertical-cavity surface-emitting laser structure

J. S. Liang, S. D. Wang, and Y. S. Huang[a)]
Department of Electronic Engineering, National Taiwan University of Science and Technology, Taipei 106, Taiwan, Republic of China

L. Malikova and Fred H. Pollak
Department of Physics and New York State Center for Advanced Technology in Ultrafast Photonic Materials and Applications, Brooklyn College of the City University of New York, Brooklyn, New York 11210

J. P. Debray, R. Hoffman, A. Amtout, and R. A. Stall
Emcore Corporation, Somerset, New Jersey 08873

(Received 8 October 2002; accepted 22 November 2002)

We have investigated a 1.3 μm InGaAlAs/InP vertical-cavity surface-emitting laser (VCSEL) structure using angle- and temperature-dependent wavelength-modulated differential surface photovoltage spectroscopy (DSPS). The DSPS measurements as functions of incident angle and temperature have been carried out in the ranges $0° \leqslant \theta \leqslant 60°$ and $300\,\mathrm{K} \leqslant T \leqslant 420\,\mathrm{K}$, respectively. Angle-dependent reflectance (R) and surface photovoltage spectroscopy (SPS) measurements have also been performed to illustrate the superior features of the DSPS technique. The differential surface photovoltage (DSPV) and SPV spectra exhibit both the fundamental conduction to heavy-hole excitonic transition of quantum well and cavity mode (CM) plus a rich interference pattern related to the mirror stacks, whereas in the R spectra only the CM and interference features are clearly visible. The energies of the excitonic transition and CM are accurately determined from the DSPV spectra. By changing the angle of incidence in the DSPS measurements the energy positions of the CM and distributed Bragg reflector features show a blueshift while the excitonic transition remains unchanged. At a fixed incident angle, the energy positions of the excitonic feature and CM show a different rate of redshift with increasing temperature, with the latter at a much slower pace. The results demonstrate considerable potential of DSPS for the nondestructive characterization of the VCSEL structures. © *2003 American Institute of Physics.*
[DOI: 10.1063/1.1538323]

I. INTRODUCTION

Vertical-cavity surface-emitting lasers (VCSELs) have optical cavities orthogonal to the conventional edge-emitting diode lasers and are attractive light sources for various applications including optical recording, optical communication, and optical computing.[1,2] VCSELs have a number of advantages compared to other existing lasers including single longitudinal mode operation, small beam divergence, low threshold current, and ease of integrability and testability.[2–4] The basic structure of a VCSEL is a Fabry–Pérot (FP) cavity consisting of an active region with embedded quantum wells (QWs), sandwiched between two multilayer distributed Bragg reflector (DBR) stacks that form highly reflecting mirrors with a broad reflectance stop band centered on a certain free space photon energy E_{Bragg}. In general, both DBR stacks are heavily p(upper)/n(lower) doped, so that the entire structure forms a p-i-n diode. The overall optical thickness of this active region determines the approximate cavity length, which is usually a few integer multiples of half of the intended lasing wavelength. Interaction of the DBRs and cavity produces a sharp FP dip in the reflection spectrum at the photon energy E_{cav}, which is usually positioned at the center of the stop band. The fundamental QW conduction to heavy-hole excitonic transition, which occurs at the energy of E_{QW}, provides the gain. To achieve the desired performance, VCSELs are designed such that E_{QW} coincides with E_{cav} at operation temperature. This means that E_{QW} at room temperature should be chosen somewhat higher than the other two so that local temperature increase during operation may compensate for the offset. In order to reduce production costs and to assure reproducibility, better means of growth and characterization need to be developed. Therefore, a contactless and nondestructive method to rapidly determine E_{QW} and E_{cav} of an epitaxial structure before laser processing is of importance to the manufacturer.

The nondestructive characterization of VCSELs presents a considerable challenge since photoluminescence,[5] a technique that has been most commonly used to characterize edge-emitting lasers, is not very useful for VCSELs because of the high DBR reflectivity. The reflectance (R) of VCSEL is determined by the physical structure of the DBRs and cavity, which yields E_{cav}, but generally provides no information on E_{QW}. Hence the R spectrum is not useful for checking the degree of mismatch between the two energies. Therefore, it will be most appropriate to explore other optical

a)Author to whom correspondence should be addressed; electronic mail: ysh@et.ntust.edu.tw

characterization techniques that are capable of extracting information on both E_{QW} and E_{cav}. Other useful optical diagnostic techniques such as contactless electoreflectance[6,7] and photoreflectance (PR)[8–15] yield, at room temperature, signals making it possible to evaluate E_{QW}, and in some cases E_{cav} as well as the built-in electric field in the *i* region from the Franz–Keldysh oscillations. Jaeger *et al.*[16] have reported room angle-dependent photocurrent (PC) spectroscopy that yields E_{QW} and E_{cav}. Huang *et al.*,[17], Liang *et al.*,[18,19] and Huang *et al.*[20] have reported surface photovoltage spectroscopy (SPS) to characterize the 980 nm InGaAs/GaAs/AlGaAs, 850 nm GaAs/GaAlAs, and 1.3 μm InGaAlAs/InP VCSELs, repectively. Recently Wang *et al.*[21] have demonstrated that angle-dependent differential surface photovoltage spectroscopy (DSPS) at room temperature can be employed to evaluate both E_{QW} and E_{cav} accurately as well as the interference pattern from the DBRs. So far, the DSPS technique offers many superior features over the other methods for VCSEL structure characterization and deserved further exploration.

In the differential surface photovoltage (DSPV) spectrum of a VCSEL structure, features of the ground state QW transition and the cavity mode (CM) can be detected simultaneously. If the signals from both features are too close to be resolved, one can increase the angle of incidence θ of the probe light to shift E_{cav} to higher energy while leaving E_{QW} unchanged. This works well as for most practical cases we have encountered, E_{cav} (θ=0°) and E_{QW} are usually quite close to each other at room temperature. An alternative approach may also be implemented through an increase of the sample temperature T at a fixed incident angle θ. This will shift E_{QW} toward lower energy region while E_{cav} will also decrease but at a slower pace.

In this article, we present detailed wavelength-modulated DSPS studies as functions of incident angle ($0° \leqslant \theta \leqslant 60°$) and temperature ($300\,K \leqslant T \leqslant 420\,K$) on a 1.3 μm InGaAlAs/InP as grown VCSEL structure. The DSPV spectra display the E_{QW} and E_{cav} as well as a rich interference pattern from DBRs. By analyzing the DSPV spectra through an appropriate line shape fit, the energy of both E_{QW} and E_{cav} may be determined accurately. The advantages of DSPS in comparison with other methods of characterizing VCSEL structures, such as SPS, PR, and PC are discussed. The results indicate that DSPS is a powerful, contactless, and nondestructive tool for characterization of wafer-scale VCSELs structures.

II. EXPERIMENT

In this study we have used a typical top-emitting VCSEL unprocessed structure with the InGaAlAs/InP based material system. The sample was grown by metalorganic chemical vapor deposition in a commercial reactor (EMCORE D 180 LDM) on an *n*-InP(001) substrate, and consisted of an active QW gain region embedded between two DBRs. The mirrors consist of 15 periods of *p*-/*n*-doped InGaAlAs high-reflectivity DBRs, each having a total thickness of 3000 nm. The active region comprised seven undoped 60 Å InGaAlAs QWs and 100 Å InGaAlAs barriers centered in InGaAlAs spacer layers, forming a single-wavelength cavity. The composition of the barriers/spacers and QWs was chosen such that the bulk band gaps were 1.127 and 0.886 eV, respectively.

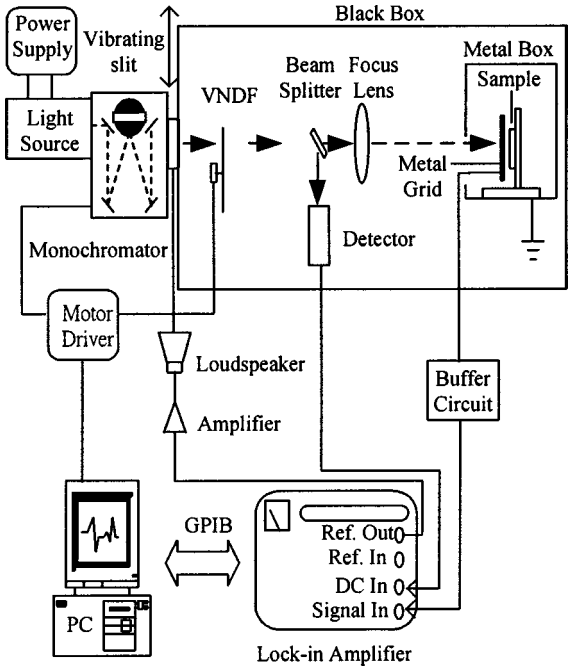

FIG. 1. Schematic diagram of the wavelength-modulated DSPS setup.

In DSPS, the derivative-like surface photovoltage is measured between the sample and a reference metal grid electrode in a capacitive manner as a function of the photon energy of the probe beam with a wavelength-modulation technique.[21–23] Figure 1 shows the schematic diagram of the wavelength modulated DSPS setup. The illumination system consisted of a 150 quartz–halogen lamp and a grating monochromator equipped with a vibrating exit slit operated by a power amplifier, employing a 2 in. loudspeaker as transducer. A beam splitter was placed in the path of the incident light. The intensity of this radiation was monitored by a power meter and was kept constant by a stepping motor connected to a variable neutral density filter, which was also placed in the path of the incident beam. The incident light intensity was maintained at a constant level of $10^{-4}\,W/cm^2$. The illumination intensity and the amplitude of wavelength modulation were experimentally selected at levels not affecting the measured spectra; typically $\Delta\lambda/\lambda_0$ was on the order of 10^{-3}. Precautions were taken to eliminate the spurious signals from light-intensity modulation. The normalized wavelength-modulated derivative-like photovoltage spectrum on the metal grid was measured with a copper plate as the ground electrode, using a buffer circuit and a lock-in amplifier. The methods of R[8–10,12–15] and SPS[17–20,24–27] have been described in the literature.

III. RESULTS AND DISCUSSION

Figure 2(a) shows the near-normal incidence reflectance (NIR) spectrum in the range of 0.8–1.2 eV. Figures 2(b) and 2(c) are, respectively, the normal-incident SPV spectrum and

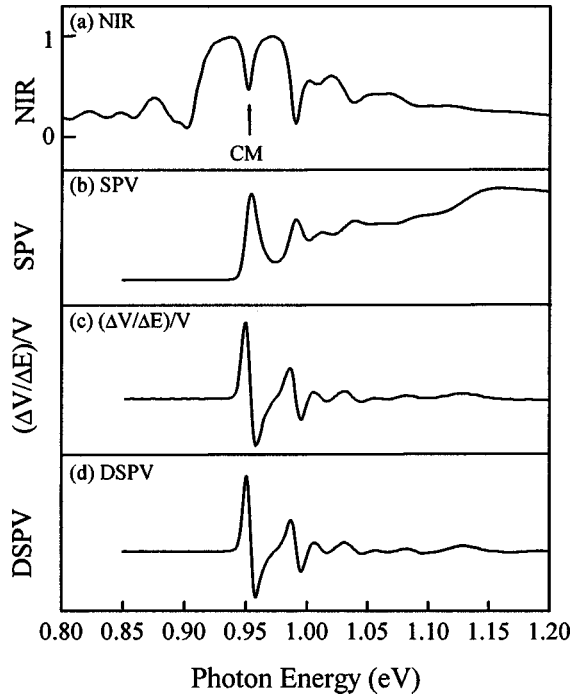

FIG. 2. (a) The near-normal incident reflectance spectrum, (b) the normal-incident SPV spectrum, (c) the numerically computed normalized first derivative of the SPV signal with respect to the photon energy, and (d) the wavelength-modulated DSPV spectrum. The arrow indicates the energy position of the cavity mode E_{cav}.

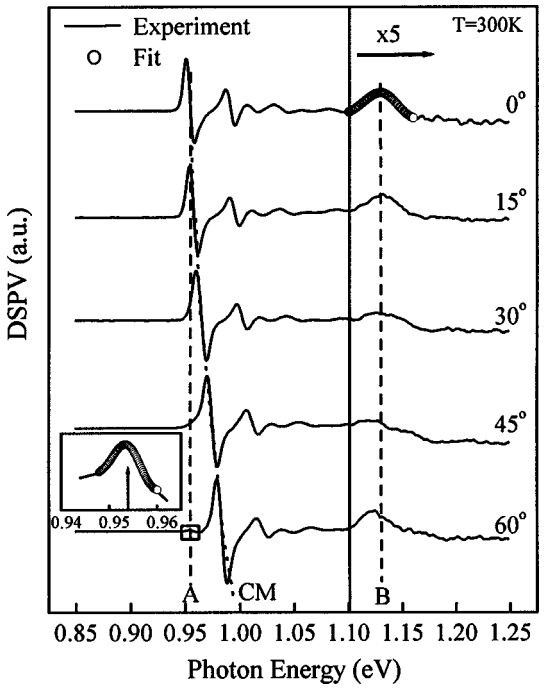

FIG. 3. Room temperature DSPV spectra for different angles of incidence θ of the light beam. The spectra are shifted vertically for clarity. With increasing θ the cavity mode and other DBR features shift to higher energy. The dotted line provides a guide to the eye for the angular dependence of the cavity mode. DSPV features denoted by dashed lines do not shift with θ which is due to the QW transition and the interband transition of the InGaAlAs barriers. The inset shows the DSPV spectrum in the range 0.94–0.965 eV for feature A at incident angle $\theta=60°$. The open circle curves are the first derivative of a Gaussian line shape fit for the 1C–1H excitonic transition and the InGaAlAs interband transition.

the numerically computed normalized first derivative of the SPV signals with respect to the photon energy $(\Delta V/\Delta E)/V$, while Fig. 2(d) is the normal-incident DSPV spectrum measured with a wavelength modulation technique. The feature at the center of the stop band at 0.952 ± 0.002 eV is the CM structure, which appeared as a dip in the NIR trace and a peak in the SPV spectrum. The features at higher energies (and lower energies for NIR) are due to interference from the DBRs. Note that the SPV peaks correspond to the NIR dips. In addition, both SPV and DSPV spectra showed a broad feature around 1.13 eV, which has its origin from the InGaAlAs barriers. Careful comparison of Figs. 2(c) and 2(d) shows that the wavelength-modulated DSPV spectrum duplicates the structural form of the numerical derivative SPV signal. The result provides direct evidence that the mechanism for the wavelength-modulated surface photovoltage of VCSEL structure is dominated mainly by energy modulation.

Figure 3 shows a set of DSPV spectra measured under different incident angles θ of the light beam at room temperature. In terms of the dependence on the incident angle θ, the observed features can be grouped into two types. Type-I features correspond to those that shift toward higher energy with increasing θ. These include the CM (dotted line) and the DBR mirror features. Type-II features (highlighted as letters A and B) show no shift at all with the incident angle. Feature A corresponds to the onset of absorption of 1C–1H transition in the InGaAlAs QWs and becomes visible at θ larger than 45° as a small peak located in the lower energy region. The inset of Fig. 3 shows the DSPV spectrum in the range of 0.94–0.965 eV, shown by the open circles is the derivative of a Gaussian line shape fit, which is appropriate for excitonic transition.[28] The obtained value for the 1C–1H transition (feature A) energy is $E_{\mathrm{QW}}=0.954\pm0.001$ eV with the broadening parameter $\Gamma=0.004\pm0.001$ eV. Feature B appears as a broad structure in Fig. 3 and is observed at higher photon energy (denoted by an arrow) at 1.13 eV. The feature corresponds to the direct gap of the InGaAlAs barriers.

Figure 4 summarizes the results of the angle-dependent DSPS, SPS, and R measurements. The open circles and closed triangles are $E_{\mathrm{QW}}(\theta)$ determined from DSPS and SPS, respectively. The values for $E_{\mathrm{cav}}(\theta)$ as determined from DSPS, SPS, and R are represented as open triangles, closed circles, and open squares, respectively. The angle independent nature of $E_{\mathrm{QW}}(\theta)$ is quite clear from DSPS and SPS measurements as illustrated in Fig. 4. The dependence of $E_{\mathrm{cav}}(\theta)$ determined from DSPS, SPS, and R spectra agree well with each other. The angular dependent $\lambda_{\mathrm{cav}}(\theta)$ can be fitted with[9,18,21]

$$\lambda_{\mathrm{cav}}(\theta)=(2d/m)(1-\sin^2\theta/n^2)^{1/2}$$
$$=\lambda(0°)(1-\sin^2\theta/n^2)^{1/2}. \quad (1)$$

In Eq. (1), m is an integer, $\lambda(0°)$ is the wavelength at normal incidence, d is the effective thickness, and n is the effective refraction index for the cavity. The effective cavity length and effective refraction index are deduced to be 3873 ± 40 Å and 3.365 ± 0.002, respectively. The value of the determined effective cavity length is in reasonable agreement with the intended number.

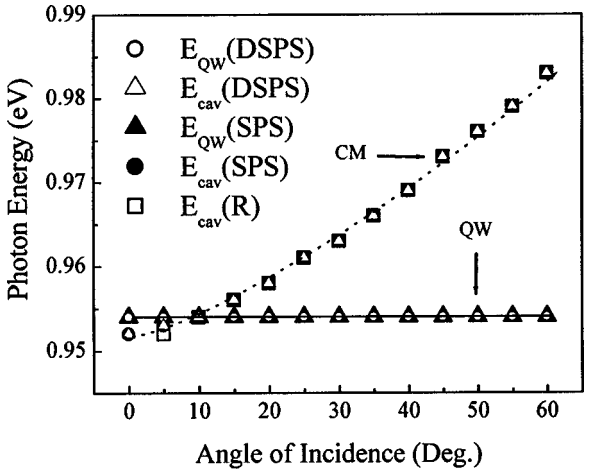

FIG. 4. Angle dependence of the fundamental excitonic quantum well transition and cavity mode determined from the SPS, DSPS, and *R* measurements. The open circles and closed triangles are $E_{QW}(\theta)$ determined from DSPS and SPS, respectively, while the open triangles, closed circles and open squares are $E_{cav}(\theta)$ determined from DSPS, SPS, and *R*, respectively. The dotted line is a least-squares fit to Eq. (1).

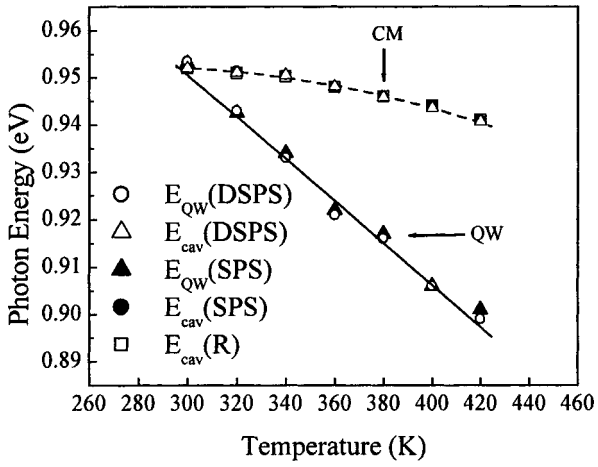

FIG. 6. Temperature dependence of the fundamental excitonic quantum well transition and cavity mode determined from the DSPS, SPS, and *R* measurements. The open circles and triangles are $E_{QW}(T)$ and $E_{cav}(T)$, respectively, as determined from DSPS. The closed triangles and circles are $E_{QW}(T)$ and $E_{cav}(T)$, respectively, as determined from SPS, while the open squares are $E_{cav}(T)$ as determined from NIR. The solid and dashed lines are least-squares fits for $E_{QW}(T)$ and $E_{cav}(T)$, respectively, in the range of 300–420 K.

Figure 5 shows representative temperature dependent DSPV spectra recorded at $\theta=60°$. The temperature range recorded is from 300 to 420 K. The feature due to the QW transition is seen to redshift with increasing temperature. The CM also shows a redshift, due to thermal expansion of the cavity and a change in index of refraction *n*, but at a much slower pace. The dashed line and dotted line are a guide to the eye showing, respectively, the paths of the temperature variation of QW transition and CM.

Figure 6 summarizes the results of the temperature-dependent DSPS, SPS, and *R* measurements. In Fig. 6, the values for $E_{QW}(T)$ and $E_{cav}(T)$ deduced from DSPS are represented as open circles and triangles, respectively, while the corresponding data from the SPS are denoted by closed triangles and circles. The open squares in Fig. 6 are $E_{cav}(T)$ data from NIR measurements. There is good agreement between the DSPS data and the relevant SPS and *R* measurements. The temperature dependence of $E_{QW}(T)$ can be expressed by a Bose–Einstein-type expression:[17,20,28]

$$E_{QW}(T)=E_{QW}(0)-2a_B/[\exp(\Theta_B/T)-1], \tag{2}$$

where $E_{QW}(0)$ is the energy at $T=0$ K, a_B represents the strength of the average electron–phonon interaction, and Θ_B corresponds to the average phonon temperature. For small temperature variations near and above room temperature, the behavior of $E_{QW}(T)$ as given by Eq. (2) is virtually linear with temperature T and can be expressed as:

$$E_{QW}(\mathrm{T})=E_{QW}(0)-2(a_B/\Theta_B)T+\ldots\approx E_{QW}(0)-\alpha T. \tag{3}$$

A least-squares fit to the linear function as given by Eq. (3) yields $\alpha=3.9\times10^{-4}$ eV/K and is shown by the solid line in Fig. 6. This value is comparable to that found for other III–V direct gap materials.[29] The quantity $E_{cav}(T)$ has been fitted to a quadratic expression, i.e., $E_{cav}(T)=E_{cav}(0)+AT+BT^2$, which gives $E_{cav}(0)=0.95$ eV, $A=-3.5\times10^{-5}$ eV/K, and $B=-1.0\times10^{-7}$ eV/K^2. The obtained values of A and B are comparable to those in Refs. 17 and 20.

The DSPS has a number of advantages over other methods such as SPS, *R*, PR, and PC. The DSPS and SPS are both related to the photovoltaic effect, which is very sensitive to the low light levels that reach the QW region through the top DBR mirrors. The wavelength-modulated DSPS yields a derivative spectrum, which can further improve the accuracy and sensitivity of the SPS dramatically. The DSPV spectrum can be fitted by a line shape function and the energies of various transitions may be evaluated to within a few milli-electron volts at room temperature. For instance, in this

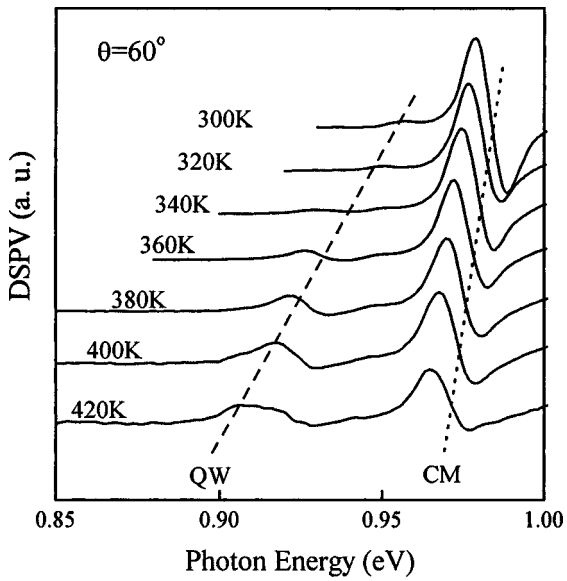

FIG. 5. Results of temperature variation ($300\,\mathrm{K}\leqslant T\leqslant 420\,\mathrm{K}$) experiments on DSPS measurements at $\theta=60°$. The dashed and the dotted curves are guides to the eye, of $E_{QW}(T)$ and $E_{cav}(T)$, respectively. The $E_{QW}(T)$ shifts to lower energy with increasing temperature, while the $E_{cav}(T)$ also shows a redshift but at a much slower pace.

study, we have also fitted structure *A*, which is observed in both the numerically computed first derivative of the SPV and DSPV spectra. Both fits give identical values for the transition energy. The broadening parameter of *A* feature for SPV is computed to be $\Gamma=0.006\pm0.001$ eV, which is somewhat larger than the DSPS measurement. While both the CM and 1C−1H transition are always observed in DSPS, for PR in some cases, only the latter is observed. In DSPS and SPS a rich interference pattern related to the properties of the DBR are observed in contrast to PR. In addition, DSPS has an advantage over PR in that it requires no pumping beam. The techniques of DSPS, SPS and PR are contactless and require no special mounting of the sample and hence are completely nondestructive and can be employed on the entire wafer. This attribute is superior to PC where contact must be made with the sample and hence some degree of damage to the sample is inevitable.

IV. SUMMARY

In summary we have performed an angle- and temperature-dependent wavelength-modulated DSPS investigation of an InGaAlAs/InP VCSEL structure. At a fixed temperature, the CM and DBR mirror features show a blueshift with increasing incident angle θ, while the QW transition remains unchanged. The energy of the QW transition and CM may be evaluated accurately through the line shape fit to the DSPV spectrum. At fixed θ, the E_{QW} shows a redshift with increasing temperature, while E_{cav} also increases but at a much slower pace than E_{QW}. The results demonstrate that the characterization of VCSEL wafers by angle- and temperature-dependent DSPS allow one to obtain detailed information about excitonic transitions and cavity properties, and hence to assess the overlap between the gain spectrum of the active QWs region and the CM in a VCSEL structure. DSPS shows a number of advantages over techniques such as SPS, PR, and photocurrent spectroscopy, which have been used to study VCSEL structures. This study demonstrates the considerable potential of DSPS for the characterization of the VCSEL structures.

ACKNOWLEDGMENTS

The authors J. S. L., S. D. W., and Y. S. H. acknowledge the support of National Science Council of the Republic of China under Project No. NSC90-2215-E-011-003. L. M. and F. H. P. acknowledge the support of Army Research Laboratory Contract No. DAAD17-99-C-0072 and the New York State Science and Technology Foundation through its Centers for Advanced Technology program.

[1] N. K. Dutta, D. T. Nichols, D. Avkshoori, D. L. Sivco, and A. Y. Cho, Appl. Phys. Lett. **67**, 588 (1995).
[2] T. C. Banwell, A. C. Von Lehmen, and R. R. Cordell, IEEE J. Quantum Electron. **29**, 635 (1993).
[3] K. Iga and F. Koyama, in *Surface Emitting Semiconductor Lasers and Arrays*, edited by G. A. Evans and J. M. Hammer (Academic, San Diego, CA, 1993), p. 71.
[4] H. Soda, K. Iga, C. Kitahara, and Y. Suematsu, Jpn. J. Appl. Phys. **18**, 2329 (1979).
[5] S. Gramlich, J. Sebastian, M. Weyers, and R. Hey, Phys. Status Solidi A **152**, 293 (1995).
[6] F. H. Pollak, H. Qiang, D. Yan, W. Krystek, and S. Moneger, Solid-State Electron. **38**, 1121 (1995).
[7] S. Moneger, H. Qiang, F. H. Pollak, D. L. Mathine, R. Droopad, and G. Maracas, Solid-State Electron. **39**, 871 (1996).
[8] P. D. Berger, C. Bru, T. Benyattou, G. Guillot, A. Chenevas-Paule, L. Couterier, and P. Grosse, Appl. Phys. Lett. **68**, 4 (1996).
[9] P. J. Klar, G. Rowland, T. E. Sale, T. J. C. Hosea, and R. Grey, Phys. Status Solidi A **170**, 145 (1998).
[10] P. J. Klar, G. Rowland, P. J. S. Thomas, A. Onischenko, T. E. Sale, T. J. C. Hosea, and R. Grey, Phys. Rev. B **59**, 2894 (1999).
[11] P. J. Klar, G. Rowland, P. J. S. Thomas, A. Onischenko, T. E. Sale, T. J. C. Hosea, and R. Grey, Phys. Rev. B **59**, 2902 (1999).
[12] P. M. A. Vicente, P. J. S. Thomas, D. Lancefield, T. E. Sale, T. J. C. Hosea, A. R. Adams, P. J. Klar, and A. Raymond, Phys. Status Solidi B **211**, 255 (1999).
[13] T. E. Sale, T. J. C. Hosea, and P. J. S. Thomas, IEEE Photonics Technol. Lett. **12**, 1328 (2000).
[14] S. A. Choulis, S. Ghosh, and T. J. C. Hosea, J. Appl. Phys. **88**, 5547 (2000).
[15] S. Ghosh, T. J. C. Hosea, and S. B. Constant, Appl. Phys. Lett. **78**, 3250 (2001).
[16] A. Jaeger, P. M. Petroff, and T. D. Lowes, Appl. Phys. Lett. **78**, 3012 (2001).
[17] Y. S. Huang, L. Malikova, F. H. Pollak, H. Shen, J. Pamulapati, and P. Newman, Appl. Phys. Lett. **77**, 37 (2000).
[18] J. S. Liang, Y. S. Huang, C. W. Tien, Y. M. Chang, C. W. Chen, N. Y. Li, P. W. Li, and F. H. Pollak, Appl. Phys. Lett. **79**, 3227 (2001).
[19] J. S. Liang, S. D. Wang, Y. S. Huang, C. W. Tien, Y. M. Chang, C. W. Chen, N. Y. Li, D. Y. Lin, and F. H. Pollak, Appl. Phys. Lett. **80**, 752 (2002).
[20] Y. S. Huang, L. Malikova, F. H. Pollak, J. P. Debray, R. Hoffman, A. Amtout, and R. A. Stall, J. Appl. Phys. **91**, 6203 (2002).
[21] S. D. Wang, J. S. Liang, Y. S. Huang, C. W. Tien, Y. M. Chang, C. W. Chen, N. Y. Li, K. K. Tiong, and F. H. Pollak, J. Appl. Phys. **92**, 2350 (2002).
[22] J. Lagowski, W. Walukiewicz, M. M. G. Slusarczuk, and H. C. Gatos, J. Appl. Phys. **50**, 5059 (1979).
[23] S. A. Tabatabaei, A. A. Iliadis, and C. E. C. Wood, J. Electron. Mater. **24**, 87 (1995).
[24] L. Kronik and Y. Shapira, Surf. Sci. Rep. **37**, 1 (1999).
[25] C. L. Balestra, J. Lagowski, and H. C. Gatos, Surf. Sci. **26**, 317 (1971).
[26] J. Lagowski, Surf. Sci. **299/300**, 92 (1994).
[27] L. Aigouy, F. H. Pollak, J. Petruzzello, and K. Shahzad, Solid State Commun. **102**, 877 (1997).
[28] F. H. Pollak and H. Shen, Mater. Sci. Eng., R. **10**, 275 (1993).
[29] *Numerical Data and Functional Relationships in Science and Technology*, edited by O. Madelung, Landolt-Bornstein, New Series, Group III, Vol. 17 (Springer, New York, 1987).

IOP PUBLISHING JOURNAL OF PHYSICS: CONDENSED MATTER

J. Phys.: Condens. Matter **19** (2007) 096009 (8pp) doi:10.1088/0953-8984/19/9/096009

Surface photovoltage spectroscopy characterization of InGaPN alloys grown on GaP substrates

H P Hsu[1], P Y Wu[1], Y S Huang[1,5], S Sanorpim[2], K K Tiong[3], R Katayama[4] and K Onabe[4]

[1] Department of Electronic Engineering, National Taiwan University of Science and Technology, Taipei 106, Taiwan
[2] Department of Physics, Faculty of Science, Chulalongkorn University, Pathumwan, Bangkok 10330, Thailand
[3] Department of Electrical Engineering, National Taiwan Ocean University, Keelung 202, Taiwan
[4] Department of Advanced Materials Science, The University of Tokyo, 5-1-5 Kashiwanoha, Kashiwa 277-8561, Japan

E-mail: ysh@mail.ntust.edu.tw

Received 22 November 2006, in final form 19 January 2007
Published 12 February 2007
Online at stacks.iop.org/JPhysCM/19/096009

Abstract

$In_{0.176}Ga_{0.824}P_{1-y}N_y$ ($y = 1.5\%$–8.7%) alloys grown on GaP(001) substrates via metalorganic vapour phase epitaxy were characterized by surface photovoltage spectroscopy (SPS) in the temperature range between 125 and 400 K. The band gap energies are determined and their temperature dependences are analysed by Varshni and Bose–Einstein expressions. The parameters that describe the temperature variations of the band gap energies are evaluated and discussed. The surface photovoltage spectra also revealed that a transition from indirect to direct band gap is taking place for the N-incorporated samples and the quadratic correction for the band gap bowing is only applicable for low nitrogen containing samples.

1. Introduction

Due to the huge band gap bowing, common in the III–(III)–V–N-type alloys [1–4], $In_xGa_{1-x}P_{1-y}N_y$ is of great interest for well materials with a large barrier height for electron confinement in lattice-matched InGaPN/GaP quantum wells (QWs) [5]. The incorporation of N into the highly compressive-strained InGaP system results in a reduction of its lattice constant, thus reducing the strain in the InGaPN layer grown on the GaP substrate. The InGaPN alloy is an alternative to the GaPAsN alloy that yields high-optical-quality QWs with the lattice-matched GaPAsN/GaP heterostructure [6]. Despite its scientific interesting, to date, only a few relevant research reports have been published [7–9]. Additionally, most studies have

[5] Author to whom any correspondence should be addressed.

employed photoluminescence (PL) spectra at low temperature; therefore, most of the electro-optical properties that have been examined have been limited to low temperatures. Detailed studies of the electro-optical characteristics at room temperature and higher temperatures are not only interesting but also necessary and important.

In this study, surface photovoltage spectroscopy (SPS) was used to characterize the $In_{0.176}Ga_{0.824}P_{1-y}N_y$ ($y = 1.5\%$–8.7%) alloys grown on GaP(001) substrates by metalorganic vapour phase epitaxy (MOVPE). The photovoltage is mainly generated in the space-charge region at the surface. The SPS characterization was made in the temperature range from 125 to 400 K. The band gap energies are determined and their temperature dependences are analysed by the Varshni expression [10] and an expression containing the Bose–Einstein occupation factor for phonons [11, 12]. The parameters that describe the temperature variations of the band gap energies are evaluated and discussed.

2. Experimental details

Four $In_{0.176}Ga_{0.824}P_{1-y}N_y$ ($y = 1.5\%$–8.7%) alloy films were grown on GaP(001) substrates by low-pressure (60 Torr) MOVPE. Trimethylgallium (TMG), trimethylindium (TMI), PH_3 and dimethylhydrazine (DMHy) were used as the source materials. After growth of a 0.3 μm-thick GaP buffer layer at 710 °C, a 0.3 μm-thick InGaPN epitaxial layer was deposited at 635 °C. The growth rate was around 1.0 μm h^{-1}. Films with various nitrogen concentrations were obtained by changing the molar flow ratio of DMHy to the total group V elements (DMHy + PH_3). The alloy compositions were determined from high-resolution x-ray diffraction and secondary ion mass spectroscopy data. For comparison purposes, an $In_{0.176}Ga_{0.824}P$/GaP sample without nitrogen was also grown and characterized.

In SPS measurement, the contact potential difference between the sample and a reference grid electrode is measured in a capacitive manner as a function of the photon energy of the probe beam by holding the grid fixed and chopping the probe beam at 200 Hz [13]. The light from a 150 W quartz–halogen lamp was passed through a PTI 0.25 m grating monochromator and focused onto the samples. It is known that, under low optical excitation, the photovoltage (PV) signal is proportional to the absorption coefficient α multiplied by the photon flux density Φ ($PV \propto \alpha\Phi$) [14, 15]. To verify that the measurements were performed under low optical excitation, the amplitude of the photovoltage near peak position was checked with various light intensities I between 5×10^{-6} and 5×10^{-4} W cm^{-2}. The results indicate that, for $I \leqslant 3 \times 10^{-4}$ W cm^{-2}, PV varies linearly with incident light intensity. Subsequently, incident light intensity maintained at a constant level of $\sim 10^{-4}$ W cm^{-2} was used for the study. A beam splitter was placed in the path of the incident light. The intensity of this radiation was monitored by a power meter and was kept constant by a stepping motor connected to a variable neutral density filter placed in the path of the incident beam. The photovoltage spectrum on the metal grid was measured with a copper plate as the ground electrode, using a buffer circuit and a lock-in amplifier. A CTI model 22 closed-cycle cryogenic refrigeration system equipped with a model 32B digital temperature controller was used for low-temperature measurements. For the high-temperature experiments, each sample was mounted on one side of a copper finger of an electric heater, which enabled one to control and stabilize the sample temperature. The measurements were made with a temperature stability of 0.5 K or better.

3. Results and discussion

Figure 1 shows the room-temperature surface photovoltage (SPV) spectra for five $In_{0.176}Ga_{0.824}P_{1-y}N_y$ samples with various nitrogen compositions of $y = 0$, 1.5%, 2.3%, 7.4%,

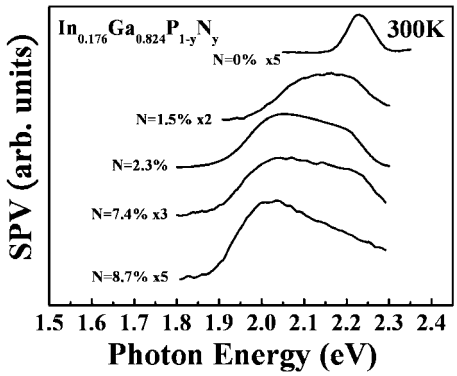

Figure 1. Surface photovoltage spectra for five $In_{0.176}Ga_{0.824}P_{1-y}N_y$ samples with various nitrogen compositions $y = 0\%$, 1.5%, 2.3%, 7.4%, and 8.7%, measured at room temperature.

and 8.7%. As described earlier in the experimental section, under low optical excitation the photovoltage signal PV is proportional to the absorption coefficient α multiplied by the photon flux density Φ ($PV \propto \alpha\Phi$) [14, 15]. The latter is equal to the light intensity I divided by the photon energy E: $\Phi = I/E$. Thus, by keeping I constant, one has $PVE \propto \alpha$. It has been reported that the band structure of $In_xGa_{1-x}P$ with indium composition $x < 0.27$ is indirect [16] and we therefore analysed the SPS spectrum for the $y = 0$ sample using the relation $(PVE)^{1/2}$ versus E. The band gap energy can be obtained by extrapolating the linear part of the plot $(PVE)^{1/2}$ versus E to zero. As shown in figure 2(a), the fit using $(PVE)^{1/2}$ versus E yields a satisfactory result which agrees well with the indirect band gap character of $In_xGa_{1-x}P$ with indium composition $x < 0.27$. The indirect band gap is determined to be 2.147 ± 0.03 eV. On the other hand, the N-containing samples exhibited direct band gap character and the SPV spectra are depicted in figure 2(b). The SPV spectra that were obtained were fitted well using the relation $(PVE)^2$ versus E, which is the characteristic of a direct band structure. The obtained band gap energy values of $In_{0.176}Ga_{0.824}P_{1-y}N_y$ alloys at room temperature are 2.002 ± 0.025, 1.935 ± 0.025, 1.922 ± 0.025, and 1.900 ± 0.025 eV for samples with nitrogen content of $y = 1.5\%$, 2.3%, 7.4%, and 8.7%, respectively. The use of SPS for the extraction of E_g is, at heart, nothing more than an emulation of an absorption spectrum. However, as opposed to transmission spectroscopy, for example, SPS does not require light collection and therefore can be performed on arbitrarily thick samples and does not require the sample to be removed from the substrate. One must bear in mind that the obtained value of E_g is only approximate.

The results indicate that incorporation of small amounts of N into $In_{0.176}Ga_{0.824}P$ changes the nature of the fundamental optical transition from an indirect-gap transition in $In_{0.176}Ga_{0.824}P$ to a direct-gap transition in $In_{0.176}Ga_{0.824}P_{1-y}N_y$ alloys. This finding is quite similar to the previous report on GaPN alloys [17] where N-induced transformation from indirect to direct gap has been explained in terms of the band anticrossing model.

A plot of energy band gap versus N concentration, obtained from room-temperature SPS measurements, for the $In_{0.176}Ga_{0.824}P_{1-y}N_y$ alloys system is displayed in figure 3. For comparison purposes, the low-temperature (10 K) PL peak energy positions [7] are also depicted in figure 3. As shown in figure 3, by increasing the N concentration from $y = 0$ to 2.3% the energy gap red-shifts by 208 meV, corresponding to a 340 meV red-shift of the PL peak. With a further increase in the N concentration, the red-shift of the band gap slows down dramatically. It is well known that the incorporation of a small amount of nitrogen in

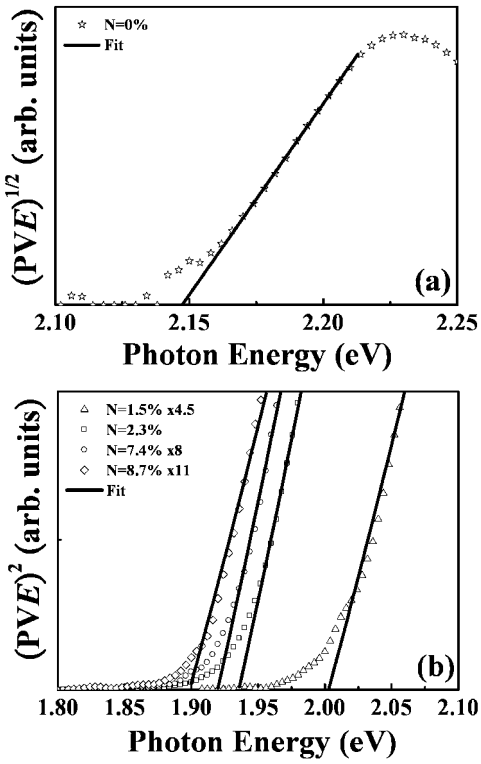

Figure 2. Spectral dependence of PV for the $In_{0.176}Ga_{0.824}P_{1-y}N_y$ alloys with (a) $y = 0\%$ displayed in coordinates $(PVE)^{1/2}$ versus E, (b) $y = 1.5\%$, 2.3%, 7.4%, and 8.7% plotted in coordinates $(PVE)^2$ versus E.

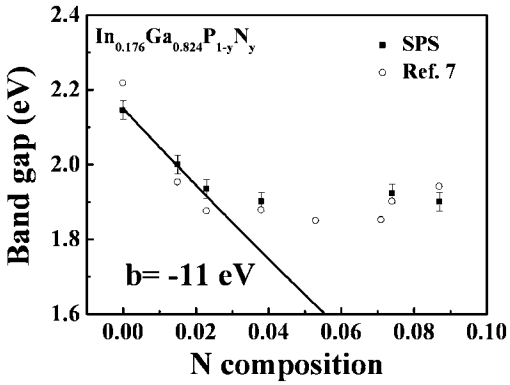

Figure 3. Band gap energy of $In_{0.176}Ga_{0.824}P_{1-y}N_y$ alloys as a function of nitrogen composition y. The solid line is the result fitted by the quadratic correction $\Delta E_g(x) = bx(x-1)$ in the range 0–2.3%. For comparison purposes, the low-temperature (10 K) PL peak energy positions taken from [7] are also shown.

III–V semiconductors such as InP [18], GaAs [19] and GaP [20] results in a strong reduction of the band gap in those materials. This behaviour is usually described well by the quadratic correction $\Delta E_g(x) = bx(x-1)$, with b being the bowing coefficient. The obtained bowing

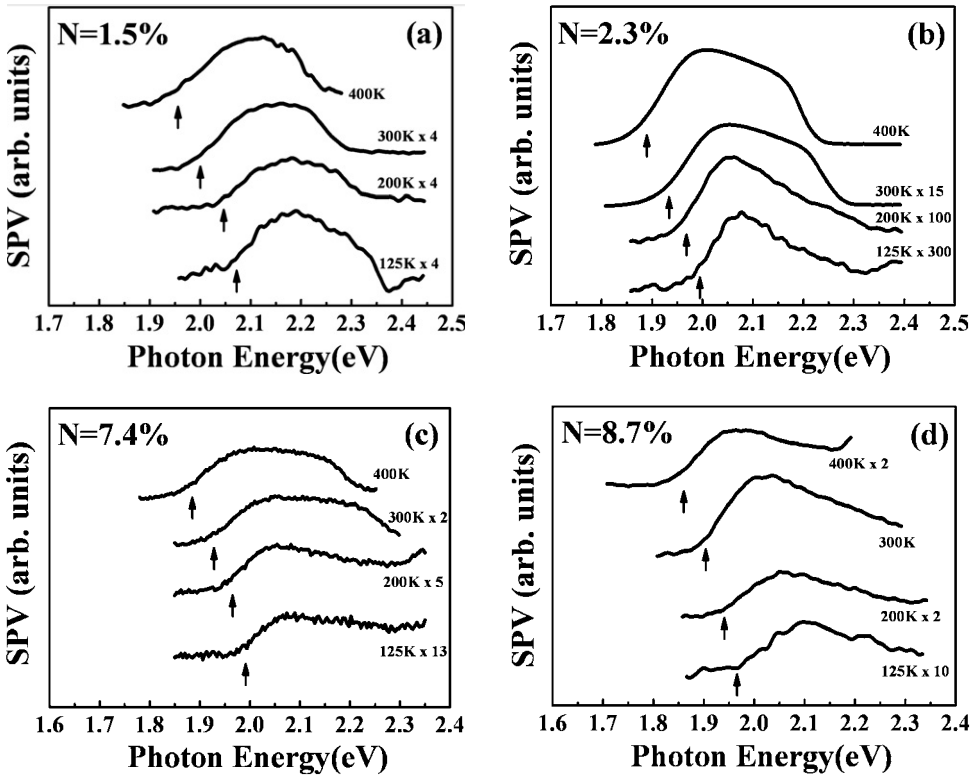

Figure 4. SPV spectra for four investigated $In_{0.176}Ga_{0.824}P_{1-y}N_y$ alloys: (a) 1.5%, (b) 2.3%, (c) 7.4%, and (d) 8.7%, at 125, 200, 300, and 400 K, respectively. The fitted band gap energy positions are indicated by arrows.

coefficient $b = -11 \pm 1$ eV for $y = 0$–2.3% is found to be smaller than the corresponding values associated with the incorporation of nitrogen in InP ($b = -16$ eV) [18] or GaP ($b = -14$ eV) [20]. For higher nitrogen content, it is noted that the quadratic correction by $\Delta E_g(x) = bx(x-1)$ is rather poor for our present experimental study. The poor agreement is not too surprising, as the quadratic model predicts a continuing increase in the red-shift, whereas the experimental evidence points to a saturation of the band gap bowing. It seems that for high nitrogen content, correction with a quadratic relationship, with the bowing parameter b being a constant, is over-simplified. The present study seems to indicate a nitrogen-concentration-dependent bowing effect [21]. Further study has been underway to include a more complete collection of N-containing InGaP materials to investigate the effect.

Displayed in figures 4(a)–(d) are the experimental SPV spectra of samples with nitrogen content $y = 1.5\%$, 2.3%, 7.4%, and 8.7% at several temperatures between 125 and 400 K. The fitted band gap energy values are indicated by the arrows. As is the case for general semiconductor properties, the band gap energies of $In_{0.176}Ga_{0.824}P_{1-y}N_y$ alloys show a red-shift with an increase in temperature. Figure 5 shows the temperature dependence of band gap energies $E_g(T)$ determined from SPS measurements for samples with nitrogen contents $y = 1.5\%$, 2.3%, 7.4%, and 8.7%. The solid lines are the least-squares fits to the Varshni semi-emprical relationship [10]:

$$E_g(T) = E_g(0) - \frac{\alpha T^2}{\beta + T}, \tag{1}$$

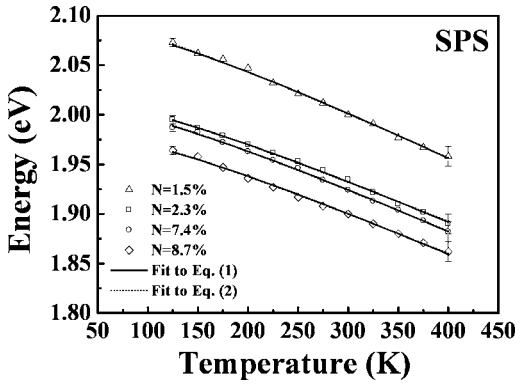

Figure 5. The temperature variations of the band gap energies for (a) 1.5%, (b) 2.3%, (c) 7.4%, and (d) 8.7%, with representative error bars. The solid curves are least-squares fits to the Varshni semi-empirical relationship and dotted curves are fitted to the Bose–Einstein-type expression.

Table 1. Values of the Varshni- and Bose–Einstein-type fitting parameters, which describe the temperature dependence of the band gap of $In_{0.176}Ga_{0.824}P_{1-y}N_y$ alloys grown on GaP, InGaPN films grown on GaAs, GaAs, GaAsN, GaP and GaPN films grown on GaP.

Samples	$E_g(0)$ (eV)	α (meV K^{-1})	β (K)	a_B (meV)	Θ_B (K)	dE_g/dT (meV K^{-1})
$In_{0.176}Ga_{0.824}P_{0.985}N_{0.015}/GaP$[a]	2.092 ± 0.005	0.51 ± 0.05	200 ± 50	56 ± 10	250 ± 50	-0.44
$In_{0.176}Ga_{0.824}P_{0.977}N_{0.023}/GaP$[a]	2.014 ± 0.005	0.48 ± 0.05	200 ± 50	53 ± 10	250 ± 50	-0.40
$In_{0.176}Ga_{0.824}P_{0.926}N_{0.074}/GaP$[a]	2.008 ± 0.005	0.47 ± 0.05	200 ± 50	52 ± 10	250 ± 50	-0.40
$In_{0.176}Ga_{0.824}P_{0.913}N_{0.087}/GaP$[a]	1.982 ± 0.005	0.46 ± 0.05	200 ± 50	51 ± 10	250 ± 50	-0.37
$In_{0.46}Ga_{0.54}P_{0.995}N_{0.005}/GaAs$[b]	1.862	0.51	255	53	250	-0.38
$In_{0.46}Ga_{0.54}P_{0.99}N_{0.01}/GaAs$[b]	1.825	0.49	255	53	250	-0.37
GaAs[c]	1.522	0.58	300			-0.50
$GaAs_{0.9703}N_{0.0297}$[d]	1.154	0.61	560			-0.31
GaP[c]	2.338	0.62	460			-0.53
$GaP_{0.919}N_{0.081}$[e]	2.870	0.54	460			

[a] This work.
[b] Reference [22].
[c] Reference [23].
[d] Reference [24].
[e] Reference [25].

where $E_g(0)$ is the band gap energy at 0 K. The constant α is related to the electron (exciton)–average phonon interaction strength and β is closely related to the Debye temperature. The obtained values of $E_g(0)$, α and β for samples with nitrogen content of $y = 1.5\%, 2.3\%, 7.4\%$, and 8.7% are listed in table 1. We have also fitted the experimental data to a Bose–Einstein expression [11, 12]:

$$E_g(T) = E_g(0) - \frac{2a_B}{[\exp(\Theta_B/T) - 1]}, \tag{2}$$

where $E_g(0)$ is the band gap energy at 0 K, a_B represents the strength of the electron (exciton)–average phonon interaction, and Θ_B corresponds to the average phonon temperature. Shown by the dotted lines in figure 5 are least-squares fits to equation (2). The obtained values for the various parameters are also given in table 1. For comparison purposes, the parameters for the band gap energies of InGaPN films grown on GaAs substrates [22], GaAs [23], GaAsN [24], GaP [23], and GaPN [25] films are also listed in table 1.

The parameter α of equation (1) can be related to a_B and Θ_B in equation (2) by taking the high-temperature limit of both expressions. This yields $\alpha = 2a_B/\Theta_B$. Comparison of the numbers presented in table 1 shows that this relation is indeed satisfied. From equation (2), it is straightforward to show that the high-temperature limit of the slope of the $E_g(T)$ versus T curve approaches a value of $-2a_B/\Theta_B$. The calculated value of $-2a_B/\Theta_B$ for band gap energy equals -0.45, -0.42, -0.42, and -0.41 meV K^{-1} for samples with nitrogen content of $y = 1.5\%$, 2.3%, 7.4%, and 8.7% respectively, which agrees well with the values of $[dE_g/dT] = -0.44$, -0.40, -0.40 and -0.37 meV K^{-1}, as obtained from the linear extrapolation of the high-temperature (200–400 K) SPS experimental data.

As shown in table 1, the parameters that describe the temperature variations of the band gap energies of $In_{0.176}Ga_{0.824}P_{1-y}N_y$ alloys are quite similar to those of InGaPN films grown on GaAs substrates. The values of α and dE_g/dT for $In_{0.176}Ga_{0.824}P_{1-y}N_y$ are smaller than that of GaP films. The results are similar to the GaAsN and GaAs compound systems, where the temperature-induced shift of the band gap energy in GaAsN is also substantially reduced by the presence of N in GaAs [24].

4. Summary

We have characterized four $In_{0.176}Ga_{0.824}P_{1-y}N_y$ ($y = 1.5\%$–8.7%) alloys grown on GaP(001) substrates via metalorganic vapour phase epitaxy using the SPS technique. The band gap transition energies of $In_{0.176}Ga_{0.824}P_{1-y}N_y$ ($y = 1.5\%$–8.7%) alloys are determined by fitting the SPV spectra. The results indicate that the incorporation of small amounts of N into $In_{0.176}Ga_{0.824}P$ changes the nature of the fundamental optical transition from an indirect-gap transition in $In_{0.176}Ga_{0.824}P$ to a direct-gap transition in $In_{0.176}Ga_{0.824}P_{1-y}N_y$ alloys. This finding is quite similar to the previous reports on GaPN alloys, where there is an N-induced transformation from indirect to direct band gap. Our results also indicate a nitrogen-concentration-dependent band gap bowing effect for these materials. The parameters that describe the temperature dependences of $In_{0.176}Ga_{0.824}P_{1-y}N_y$ alloys are similar to those of InGaPN films grown on GaAs substrates and smaller than that of GaP. This has been attributed to the incorporation of nitrogen into the InGaPN alloys.

Acknowledgment

The authors are grateful to acknowledge financial support from the National Science Council of Taiwan via grant no. NSC 95-2221-E-011-171.

References

[1] Xin H P, Tu C W, Zhang Y and Mascarenhas A 2000 *Appl. Phys. Lett.* **76** 1267
[2] Chtourou R, Bousbih F, Ben Bouzid S, Charfi F F, Harmand J C, Ungaro G and Largeau L 2002 *Appl. Phys. Lett.* **80** 2075
[3] Chen T H, Huang Y S, Lin D Y and Tiong K K 2004 *J. Appl. Phys.* **96** 6298
[4] Odnoblyudov V A and Tu C W 2006 *Appl. Phys. Lett.* **89** 111922
[5] Kaewket D, Tungasmita S, Sanorpim S, Nakajima F, Nakadan N, Kimura T, Katayama R and Onabe K 2007 *J. Cryst. Growth* **298** 531
[6] Biwa G, Yaguchi H, Onabe K and Shiraki Y 1998 *J. Cryst. Growth* **195** 574
[7] Sanorpim S, Nakajima F, Katayama R, Nakadan N, Kimura T, Onabe K and Shiraki Y 2003 *Phys. Status Solidi* c **0** 2773
[8] Sanorpim S, Nakajima F, Nakadan N, Kimura T, Katayama R and Onabe K 2005 *J. Cryst. Growth* **275** e1017
[9] Imanishi T, Wakahara A, Kim S M, Yonezu H and Furukawa Y 2005 *Phys. Status Solidi* a **202** 854

[10] Varshni Y P 1967 *Physica* **34** 149
[11] Lautenschlager P, Garriga M and Cardona M 1987 *Phys. Rev.* B **36** 4813
[12] Lautenschlager P, Garriga M, Logothetidis S and Cardona M 1987 *Phys. Rev.* B **35** 9174
[13] Huang Y S, Malikova L, Pollak F H, Shen H, Pamulapati P and Newman P 2000 *Appl. Phys. Lett.* **77** 37
[14] Kronik L and Shapira Y 1999 *Surf. Sci. Rep.* **37** 1
[15] Dumitras Gh, Riechert H, Porteanu H and Koch F 2002 *Phys. Rev.* B **66** 205324
[16] McGill L, Wu J W and Fitzgerald E A 2004 *J. Appl. Phys.* **95** 7561
[17] Xin H P, Welty R J and Tu C W 2000 *Appl. Phys. Lett.* **77** 1946
[18] Bi W G and Tu C W 1996 *J. Appl. Phys.* **80** 1934
[19] Pozina G, Ivanov I, Monemar B, Thordson J V and Andersson T G 1998 *J. Appl. Phys.* **84** 3830
[20] Baillargeon J N, Cheng K Y, Hofler G E, Pearah P J and Hsieh K C 1992 *Appl. Phys. Lett.* **60** 2540
[21] Bi W G and Tu C W 1997 *Appl. Phys. Lett.* **70** 1608
[22] Hsu H P, Huang Y S, Wu C H, Su Y K, Juang F S, Hong Y G and Tu C W 2004 *J. Phys.: Condens. Matter* **16** S3245
[23] Panish M B and Casey H C Jr 1969 *J. Appl. Phys.* **40** 163
[24] Uesugi K, Suemune I, Hasegawa T, Akutagawa T and Nakamura T 2000 *Appl. Phys. Lett.* **76** 1285
[25] Buyanova I A, Izadifard M, Chen W M, Xin H P and Tu C W 2006 *J. Phys.: Condens. Matter* **18** 449